Applied Catalysis B: Environmental 115–116 (2012) 149–158

Contents lists available at SciVerse ScienceDirect

Applied Catalysis B: Environmental

journal homepage: www.elsevier.com/locate/apcatb

Preparation, characterization and photocatalytic activity of TiO_2–ZrO_2 binary oxide nanoparticles

Ayca Kambur, Gulin Selda Pozan*, Ismail Boz

Istanbul University, Faculty of Engineering, Chemical Engineering Department, Avcilar, 34320, Istanbul, Turkey

ARTICLE INFO

Article history:
Received 5 August 2011
Received in revised form 5 December 2011
Accepted 9 December 2011
Available online 17 December 2011

Keywords:
Photocatalysis
Phenol
ZrO_2
TiO_2
UV irradiation
Characterization

ABSTRACT

TiO_2–ZrO_2 binary oxide catalysts were successfully prepared by a solid state reaction. The interaction between TiO_2 and ZrO_2 affected the photocatalytic efficiency of mixture. 50%TiO_2–ZrO_2 photocatalyst exhibited much higher photocatalytic activity than pure TiO_2 and the standard Degussa TiO_2 P-25 in the degradation of phenol under UV irradiation. The profound effect of binary oxide catalyst for phenol degradation is generally considered due to the high surface area, small particle size, anatase phase and high monoclinic phase of ZrO_2 content, and the presence of more surface OH groups than that of the pure TiO_2 and ZrO_2 photocatalyst. A natural pH of 5 is favorable for the photodegradation of phenol by 50TiO_2–ZrO_2 solid state dispersion (SSD) and 90% TOC removal can be achieved in 90 min. Monoclinic form of ZrO_2 is found to be more effective for photodegradation. The catalytic activity was affected by the preparation method. The observed photodegradation activity for phenol follows the order 50%TiO_2–ZrO_2 (solid state dispersion) >50%TiO_2–ZrO_2 (impregnation (IMP)) >50%TiO_2–ZrO_2 (sol–gel (SG)).

© 2011 Elsevier B.V. All rights reserved.

1. Introduction

Photocatalysis has come about as an alternative technique to decontaminate phenolic wastewaters [1] because complete mineralization has been successfully achieved under a variety of conditions [2,3].

Traditional methods to remove organic chemicals from effluents include the use of adsorbents (activated carbon, zeolites, etc.), thermal destruction, and biodegradation. These methods suffer the drawbacks of simply transferring the pollutant from one phase to another (e.g., adsorption), large energy requirements (e.g., thermal destruction), or requiring long period of treatment (e.g., biological treatment).

Photocatalytic degradation with TiO_2 provides a cost-saving alternative method for removing organic substrates from waste water [4–6]. Under UV irradiation, TiO_2 is photoactivated, and reactive species, such as, hydroxyl radicals are formed on the surfaces of the TiO_2 crystal. Most organic compounds can be mineralized through the attack of the hydroxyl radicals. Numerous studies have been carried out to improve the photocatalytic activity of TiO_2 by doping with various transition metal ions [7–9]. The results suggested that the activity of transition metal ion doped TiO_2 has a complicated relationship with the dopant concentration, the d electronic configuration, and the distribution of the dopant, etc. [10,11].

Up to present, the mechanism of transition metal ion doping of TiO_2 has not been well understood. Some $Ti_{1-x}Zr_xO_2$ materials, synthesized by a citric acid complexing method or an inverse microemulsion method, have been reported to exhibit improved photocatalytic activity for the degradation of organic pollutants in the gas phase [12]. In these works, Zr ions were mainly doped in the surface layer of TiO_2, and the higher surface acidity or the creation of surface defects was proposed as the possible reason for the improvement in the photocatalytic performance.

However, improving the quantum efficiency of the TiO_2 is still a major challenge since most of the photo-formed electrons and holes undergo recombination without utilizing them for redox reactions and which lowers the quantum yield.

ZrO_2 and ZrO_2–TiO_2 binary oxides catalysts have been investigated for their catalytic properties with organic compounds, especially for the degradation reactions in environmental remediation [13–17]; however, more information on the mechanisms behind the reactions, especially their photocatalytic properties, is necessary to improve efficiency. ZrO_2 has been used not only as a support for TiO_2 but also with TiO_2 as a binary oxide catalyst since ZrO_2 itself can act as a photocatalyst. It has been reported that the addition of small amounts of ZrO_2 into TiO_2 can decrease the particle size of TiO_2 due to the dissimilar nuclei, coordination geometry and increase in the surface area [18]. In addition to the particle size and surface area, the surface acidity in the form of OH groups is also high in binary oxide ZrO_2–TiO_2 catalysts. The OH group is trapped by the holes and suppresses the recombination process redox reactions and which suppresses the quantum yield.

* Corresponding author. Tel.: +90 212 473 70 70x17789.
E-mail address: gpozan@istanbul.edu.tr (G.S. Pozan).

0926-3373/$ – see front matter © 2011 Elsevier B.V. All rights reserved.
doi:10.1016/j.apcatb.2011.12.012

In the present work, we report the synthesis and characterization of ZrO_2–TiO_2 binary oxide nanoparticles and the influence of different preparation method, such as, solid state dispersion (SSD), impregnation (IMP) and sol–gel (SG) method on the photocatalytic degradation reaction. In addition, we have focused on the effects of different amounts of ZrO_2 as well as on the physicochemical characteristics of binary oxide catalysts and their catalytic reactivity for the degradation of the hazardous compound, phenol.

2. Experimental

2.1. Materials

Titanium tetrachloride (≥99%), zirconium(IV) oxynitrate hydrate, zirconium isopropoxide, phenol, hydroquinone, catechol, ammonia solution (25% in water), ethanol (absolute), methanol (for HPLC, ≥99%) and P25 (consisting of 75% anatase and 25% rutile with a specific BET-surface area of 50 m^2/g and primary particle size of 20 nm) were purchased from the Fluka Company and used without further purification. Deionized (D.I.) water was used for the preparation of all the catalysts as well as to dilute the phenol solution.

2.2. Catalyst preparation

Pure TiO_2 was prepared by sol–gel method. 1.5 mL $TiCl_4$ was slowly added dropwise into 15 mL ethanol solution at room temperature. A large amount of HCl gas was exhausted during the mixing process. Then, a light yellow solution was obtained and gelatinized for several days to form sol–gel. Finally, the gel was dried in the oven at 105 °C for one day, ground into fine powder, and calcined at 600 °C for 4 h.

ZrO_2 was prepared by co-precipitation. An appropriate amount of zirconium (IV) oxynitrate hydrate was dissolved in deionized hot water and the resulting solution was heated up to 65 °C. This mixture was precipitated by gradually adding NH_3 solution (25 wt%) until pH value reached at 10. The resultant solution was slowly stirred for 2 h at 65 °C. After that, solution was irradiated under 500 W microwave for 3 min. The precipitate was then filtered, washed with deionized water and dried at 100 °C for 20 h and calcined at 500 °C for 5 h.

2.3. Synthesis of TiO_2–ZrO_2 binary oxide photocatalyst

TiO_2–ZrO_2 binary oxide catalysts were prepared by solid state dispersion method. SSD initially involves mixing of TiO_2 and ZrO_2 thoroughly using ethanol in agate pastle and mortar, the solvent was then removed by evaporation while mixing. Samples prepared by this method were dried at 110 °C and calcined at 450 °C for 6 h to obtain TiO_2–ZrO_2 binary oxide catalysts. The resultant binary oxide was ground at a constant vibration rate of 300 rpm for 15 min in a Retsch MM 200 vibrant-ball mill by 12 mm ZrO_2 milling ball in ZrO_2 milling container. TiO_2 loading of the catalysts was nominally 20, 30, 50, 70 and 90 wt% and reported as the weight percentage. For instance, 20TiO_2–ZrO_2 means that the catalyst contained nominally 20% TiO_2 by weight.

In addition, 50%TiO_2–ZrO_2 catalyst prepared by sol–gel and impregnation method to compare the effect of preparation method on the photocatalytic degradation reaction.

0.05 M titanium tetrachloride was prepared by dissolving in hexan. The solution was impregnated on ZrO_2. The impregnated support was dried at 105 °C for 16 h and calcined at 600 °C for 6 h.

TiO_2–ZrO_2 was synthesized by using zirconium isopropoxide and titanium tetrachloride as starting material maintaining TiO_2:ZrO_2 ratio at 50:50 wt% at the preparation stage. In a typical preparation, 1.5 mL titanium tetra chloride was mixed with 15 mL ethanol. After magnetically stirring for 1 h, a desired stoichiometric amount of zirconium propoxide solution was added to the solution. The mixture was stirred to evaporate the solvent at room temperature and it turned into gel after stirring for 48 h. The gel was dried in the oven at 105 °C, ground into fine powder and calcined at 600 °C for 4 h to obtain the final products.

Table 1
Theoretical and ICP-mass value of wt% ratio of pure TiO_2 and ZrO_2 present in TiO_2–ZrO_2 binary oxide catalysts.

Catalyst	Theoretical value	ICP-mass value
TiO_2:ZrO_2	10 wt% ZrO_2	9.50
TiO_2:ZrO_2	50 wt% ZrO_2	49.90

2.4. Catalyst characterization

The composition of the catalyst was determined using Thermo Elemental X Series ICP-MS. Actual metal concentrations were listed in Table 2.

Powder X-ray diffractions of samples were obtained using a Rigaku D/Max-2200 diffractometer with the CuKα (λ = 1.540) radiation. Samples were scanned from 10 to 80 at a rate of 2°/min (in 2θ). The sizes of the crystalline domains were calculated by using the Scherer equation, $t = C\lambda/B\cos\theta$, where λ is the X-ray wavelength (A°), B is the full width at half maximum, θ is Bragg angle, C is a factor depending on crystallite shape (taken to be one), and t is the crystallite size (A°).

The surface OH groups of the photocatalysts were determined by FTIR spectroscopy using KBr in the form of pellets (PerkinElmer Precisely Spectrum One).

The Raman active modes of the binary mixed oxide catalysts were also investigated using Raman Spectroscopic analysis (Thermo Fisher Scientific, Nicolet Spectrometer 6700).

The BET surface areas of the samples were determined by nitrogen adsorption–desorption isotherm measurement at 77 K (Costech sorptometer 1042). The samples were degassed at 200 °C prior to the actual measurements.

The morphology and size distribution of the photocatalysts were recorded by scanning electron microscopy (JEOL/JSM-6335F) and transmission electron microscopy (JEOL HRTEM 2100). Diffuse reflectance spectra were obtained using an Ocean Optics DH-2000 BAL (UV–vis–NIR). $BaSO_4$ was used as the reflectance standard in the experiments.

2.5. Evaluation of photocatalytic activity

The photoactivity studies were carried out at atmospheric pressure and room temperature (298 K). In a typical experiment, 100 mg catalyst was dispersed in 50 mL phenol solution of initial concentration 25 mg/L and neutral pH (pH 5) under magnetic stirring.

Phenol photooxidation runs were done with quartz batch-photoreactor of cylindrical shape. LUZCHEM LZC-5 photoreactor system was used in all experiments. The light source used was 64 W UV-B lamp (LUZCHEM LZC-UVB). UV-B lamp has maximum light intensity at 312 nm and the illumination distance is 18 cm from the target. The light intensity of UV lamp used for degradation experiments was recorded with an UV/visible powermeter (Smart Sensor-AR823). The photoreactor system had a magnetic stirrer and it was used to achieve uniform conditions in the reacting mixture. Before the UV light was turned on, the solution was stirred for 60 min to ensure good adsorption equilibrium between the catalyst and the solution. After irradiation for 5 h, the phenol solution was filtered through a membrane filter (pore size 0.45 mm) and the filtrate was used for TOC measurement with a TOC-V, Shimadzu equipment. To investigate the influence of pH and inorganic anions

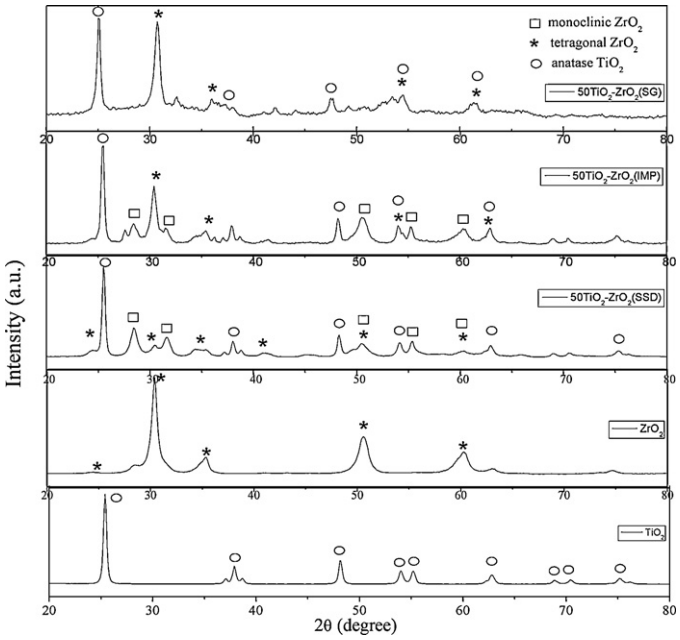

Fig. 1. XRD patterns of TiO_2, ZrO_2 and $50TiO_2$–ZrO_2 binary oxide catalysts varied with different preparation method.

on the photocatalytic reaction, all the conditions were kept constant except that inorganic anions were added at a concentration of 1×10^{-5} mol/L, or HNO_3/NaOH solutions were added to adjust the pH of phenol solution. The concentration of phenol and products were analyzed by HPLC (Thermo Finnigan) equipped with C-18 column. The mobile phase used in HPLC was a mixed solvent of methanol and water (70/30, v/v) with a flow rate of 1 mL/min.

3. Results and discussion

3.1. Catalyst characterization

The actual weight percentages of the catalysts (TiO_2 and ZrO_2) in the binary oxide catalysts were obtained by ICP-MS analysis and are reported in Table 1. The calculated wt% of the catalysts and the ICP-MS values were almost similar. Furthermore, ICP-MS values of the two representative catalysts clearly suggest that there may not be any noticeable differences between the calculated values and ICP values for the other weight percentages of TiO_2 and ZrO_2.

The BET surface areas for different catalysts are also shown in Table 2. The surface area of prepared ZrO_2 and TiO_2 are 96 and 40 m^2/g, respectively. For the TiO_2–ZrO_2 series, surface areas are decreasing with the increase in TiO_2 content. However, the surface area increased with an increase in the amount of ZrO_2. And as it is seen from Table 2, the surface area of the $50TiO_2$–ZrO_2 catalyst prepared by SSD method is higher than the catalysts prepared by impregnation and sol–gel method.

The crystallite sizes of the catalysts are calculated according to the Scherrer formula and the results are listed in Table 2.

The XRD patterns of the catalysts are shown in Fig. 1. Peaks appearing at 2θ: 25.4, 37.0 37.9, 38.6, 47.9, 54.0, 55.2, 62.9, 68.9, 70.4, 75.2, 76.2, 83.1 correspond to the diffraction patterns of (1 0 1), (1 0 3), (0 0 4), (1 1 2), (0 0 0), (1 0 5), (2 1 1), (2 0 4), (1 1 6), (2 2 0), (2 1 5), (3 0 1) and (2 2 4), respectively of the pure anatase phase of TiO_2.

XRD patterns of pure ZrO_2 show peaks appearing at 2θ: 30.02, 35.0, 50.41 and 60.0 corresponding to the diffraction patterns of (1 0 1), (0 0 2), (1 1 2) and (2 1 1), respectively of the pure tetragonal phase of ZrO_2 (Fig. 1).

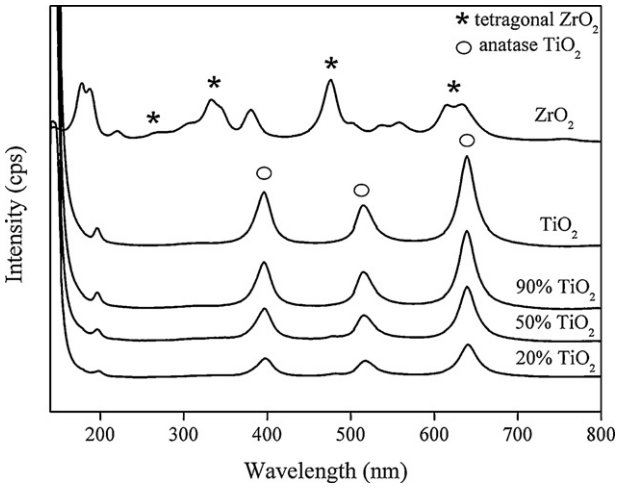

Fig. 2. Raman spectra of TiO_2–ZrO_2 binary oxide catalysts.

Moreover, a mixture of monoclinic and tetragonal zirconia catalyst, predominantly in monoclinic phase was obtained after preparation and calcination process. These XRD patterns are similar to a study by Wu et al. [15]. The characteristic peaks appear at 2θ: 24.4, 28.52, 31.5, 35.4, 41, 45, 50.4, 55.8 and 60.0 for 20–90 wt% TiO_2 to ZrO_2, corresponding to the diffraction patterns of (0 1 1), (1 1 1), (1 1 1) (2 1 1), (1 1 2) and (1 3 0) of the monoclinic phase of ZrO_2. And also, at the same calcination temperature, the Zr-doped TiO_2 materials exhibit decreasing crystallinity with increasing Zr content [15]. Vishwanathan et al. have reported that 10 wt% TiO_2 did not contribute to any change in the morphology of the binary oxide catalysts, i.e., highly crystalline particles exist [13] but, in this study, 20 wt% TiO_2 changed the morphology of the ZrO_2 in the binary oxides in which the mixed monoclinic and tetragonal phases of the ZrO_2 microcrystals are observed.

The diffraction patterns of $50TiO_2$–ZrO_2 binary oxide catalysts of different preparation methods were shown in Fig. 1. In addition to anatase TiO_2, only tetragonal zirconia phase were detectable in X-ray diffraction pattern of the $50TiO_2$–ZrO_2(SG) catalyst. It is clearly seen that the higher monoclinic phase of ZrO_2 was observed in the $50TiO_2$–ZrO_2(SSD) catalyst.

In order to confirm the formation of both tetragonal and monoclinic phases of ZrO_2, Raman spectra analysis was carried out, and the results are presented in Fig. 2. The peaks identified at around 270, 328, 470 and 650 cm^{-1} are characteristic peaks of tetragonal ZrO_2 [15]. After 20 wt%TiO_2 loading, only anatase phase of TiO_2 was present in the Raman spectra. All of the main peaks for ZrO_2, both tetragonal as well as monoclinic, were not identifiable in the Raman spectra due to the existence of high intensity anatase peaks and overlap with the ZrO_2 peaks, as shown in Fig. 2.

Amounts of monoclinic and tetragonal phase were calculated by Toyaras method [19]. These results revealed that TiO_2–ZrO_2 binary oxides exhibited mixed tetragonal and monoclinic phases of ZrO_2. In addition, our XRD observations clearly show that the phase formation in different amounts (tetragonal and monoclinic ZrO_2 phases) is governed by the method of preparation. As shown in Table 2, the tetragonal phase is observed only $50ZrO_2$–TiO_2(SG) catalyst prepared sol–gel method.

Fig. 3 shows the enlarged anatase (1 0 1) diffraction peak of the TiO_2–ZrO_2 binary oxide catalysts and TiO_2. It can be seen that this peak gradually shifts to lower angle with increasing ZrO_2 content until ZrO_2 percentage reaches to 70%. According to the Bragg's law, the decrease in 2θ values indicates the increment of the distance between crystal planes, which is in close relationship with the lattice parameters. The enlargement of lattice parameters suggest that

Table 2
The crystallite sizes, specific surface areas, band gap, morphology of materials and phenol degradation efficiencies over 90 min (%).

Catalyst	Crystallite size (nm)	S_{BET} (m^2/g)	Band gap (eV)	Morphology	Phenol degradation efficiencies over 90 min (%)
TiO_2	43	40	3.09	Anatase	88
ZrO_2	7	96	4.59	Tetragonal	22
20 wt% TiO_2	20	85	3.25	Anatase 64.9 (Vm) 35.1 (Vt)	89
30 wt% TiO_2	23	77	3.21	Anatase 78.6 (Vm) 21.4 (Vt)	100
50 wt% TiO_2 (SSD)	28	66	3.18	Anatase 83.8 (Vm) 16.2 (Vt)	100
70 wt% TiO_2 (SSD)	36	49	3.17	Anatase 69.3 (Vm) 30.7 (Vt)	60
90 wt% TiO_2	40	48	3.10	Anatase 61.6 (Vm) 38.4 (Vt)	56
50 wt% TiO_2 (IMP)	35	42	3.15	Anatase 45.7 (Vm) 54.3 (Vt)	53
50 wt% TiO_2 (SG)	72	51	3.11	Anatase 100 (Vt)	35
Degussa	32	50	3.12	Anatase	85

Vm: Monoclinic phase volume of ZrO_2 (%).
Vt: Tetragonal phase volume of ZrO_2 (%).

Zr ions are incorporated into the lattice of TiO_2 and substitute for lattice Ti ions considering the larger ionic radius of Zr ion (0.072 nm) than that of Ti ion (0.065 nm) [20,21].

The morphology and particle size of TiO_2 calcined at 600 °C, $50TiO_2$–ZrO_2 binary oxide and pure ZrO_2 calcined at 450 °C were observed by TEM in Fig. 4a–c, respectively. The average particle size of pure TiO_2 is around 65 nm in irregular sizes and shapes as shown in Fig. 4a, whereas, $50TiO_2$–ZrO_2 binary oxide catalyst possesses very small and uniform size particles of up to 30 nm in comparison to pure TiO_2. The particle size of pure ZrO_2 was also found to be around 6 nm. These results are in good agreement with XRD data.

Fig. 5 shows the SEM photograph of $50TiO_2$–ZrO_2 catalyst prepared by different preparation method. A uniform shape and size was obtained by SSD method. Agglomeration is seen in the SEM photograph of catalyst prepared by impregnation method. The morphology of the catalyst prepared by sol–gel method is different from impregnation and SSD methods. The primary particles exhibit irregular sizes and shapes. The distribution of particle size seems to be wider than those of other samples.

The impact of Zr doping on the band gap of TiO_2 was investigated using UV–vis diffuse reflectance spectroscope and the results are shown in Fig. 6. Corresponding calculated band gap values are also reported in Table 2. The calculated band gap of pure ZrO_2 is 4.59 eV, whereas the band gap is lowered to 3.25 eV by the addition of 20 wt% TiO_2. The band absorptions of the TiO_2–ZrO_2 samples shift to longer wavelengths gradually with the increment of Ti content. The estimated band gaps of the catalysts containing 20, 30, 50, 70 and 90% TiO_2 are 3.25, 3.21, 3.18, 3.17 and 3.10 eV. The band gap of TiO_2 is about 3.09 eV. It has been suggested that the quantum size effect can induce such a blue shift of band absorption [22].

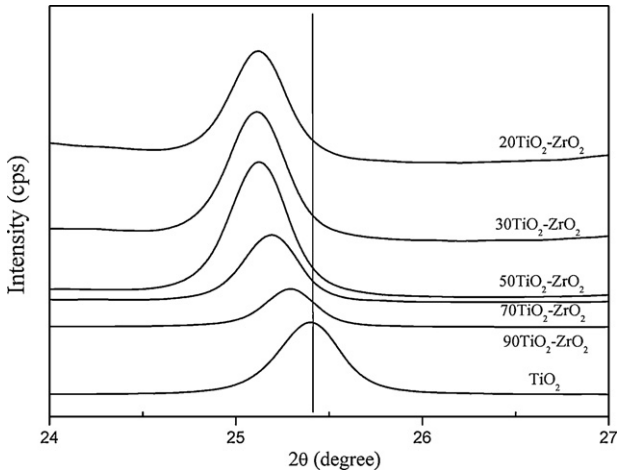

Fig. 3. The anatase (1 0 1) diffraction peak of the TiO_2–ZrO_2 binary oxide catalysts and TiO_2.

The average crystallite size (particle size) of the binary oxide catalysts also decreases from 40 to 20 nm whereas the corresponding band gap increases from 3.10 to 3.25 eV by the addition of ZrO_2 to TiO_2 (Table 2). At the same time, the particle size of the binary oxide catalysts increases with an increase in the amount of TiO_2 to ZrO_2 (Table 2), showing good accordance with the DRS spectra Fig. 6.

In addition, the average particle size and band gap of the $50TiO_2$–ZrO_2 binary oxide catalyst varied with different preparation method. As shown in Table 2, the lowest particle size (28 nm) and the highest band gap energy (3.18 eV) were obtained with the $50TiO_2$–ZrO_2(SSD) binary oxide catalyst prepared by solid state dispersion method.

Photocatalyst samples were also analyzed by FTIR spectroscopy. FTIR spectra of samples showed O—H functional group and the bands at 3350 cm^{-1} and 1620 cm^{-1} represent the surface-adsorbed water and hydroxyl group [23]. Pure TiO_2 did not show any peaks at around 3350 cm^{-1} and 1620 cm^{-1} corresponding to the OH group in the FTIR spectra (FTIR spectra is not shown here). No peaks, therefore, corresponding to the OH group appears in FTIR spectra. On the other hand, for 10 wt% ZrO_2 on the TiO_2 binary oxide catalysts, small peaks appearing at 3330 was observed while the band at 1620 cm^{-1} was not apparent. The concentration of the hydroxyl groups was measured as the integrated areas of corresponding peaks.

The concentration of the hydroxyl groups was increased with increase in the wt% of ZrO_2 to TiO_2. However, the peak area was decreased after 50 wt%ZrO_2 loading. On the other hand, the concentration of the peaks increased with an increase in the TiO_2 loading to ZrO_2 up to 50 wt% and decreased with the further addition of TiO_2. Furthermore, the peaks identified at 3350 and 1620 cm^{-1} correspond to the stretching and bending modes of molecularly adsorbed water [24]. This result indicated that the higher catalytic activity of $50TiO_2$–ZrO_2 was attributed to a higher concentration of the hydroxyl groups of $50TiO_2$–ZrO_2.

3.2. Reaction mechanism and kinetics

In general, the diffusion rate of adsorbed reactive species on the surface is faster than the photocatalytic reaction rate. Therefore, the photocatalytic reaction is the rate control step. The photocatalytic degradation can be described with the Langmuir–Hinshelwood equation [25]:

$$\frac{1}{r_0} = \frac{1}{k_r K_{ads} c_0} + \frac{1}{k_r}$$

Table 3
Reaction rate constant (k_r), adsorption equilibrium constant (K_{ads}) and correlation coefficient (R^2) in the photocatalytic degradation of phenol.

Catalyst	k_r (mg L^{-1} min^{-1})	K_{ads} (mg^{-1} L)	R^2
TiO_2	0.54	0.212	0.982
10 wt% ZrO_2	0.21	0.253	0.945
30 wt% ZrO_2	0.27	0.288	0.933
50 wt% ZrO_2	0.73	0.360	0.991
ZrO_2	0.08	0.712	0.953
20 wt% TiO_2	0.25	0.433	0.962
30 wt% TiO_2	0.51	0.371	0.991
50 wt% TiO_2 (SSD)	0.73	0.360	0.994
Degussa P-25	0.62	0.313	0.972
50 wt% ZrO_2/TiO_2 (IMP)	0.18	0.342	0.905
50 wt% ZrO_2/TiO_2 (SG)	0.14	0.364	0.917

where r_0 is the initial reaction rate (mg L^{-1} min^{-1}), k_r is the Langmuir–Hinshelwood reaction rate constant (mg L^{-1} min^{-1}) and K is the Langmuir adsorption constant (L mg^{-1}).

In Table 3 are the values of the adsorption equilibrium constant (K_{ads}), the reaction rate constant (k_r) and correlation coefficient (R^2) determined by linear regression. It is visible that ZrO_2 shows a higher adsorption equilibrium constant than TiO_2 due to the higher surface area of ZrO_2. On the other hand, TiO_2 exhibits a higher rate constant.

For the TiO_2–ZrO_2 binary oxide catalysts the adsorption equilibrium constant is consistently increased with an increase in the amount of ZrO_2 loadings to TiO_2. It can be explained in terms of increased specific surface area. However, the adsorption equilibrium constants are consistently decreased with an increase in the amount of TiO_2 loadings to ZrO_2. In addition, highest reaction rate (0.73 mg L^{-1} min^{-1}) were obtained with the 50TiO_2–ZrO_2(SSD) binary oxide catalyst. One explanation lies in the strong interaction between the TiO_2 and ZrO_2. After 50 wt%TiO_2 loading, reaction rate constant is decreased.

The photocatalytic degradation performance for TiO_2, ZrO_2 and TiO_2–ZrO_2 binary oxide catalyst prepared by SSD method were monitored for the oxidative degradation of phenol and the results are shown in Fig. 7.

The photocatalytic degradation performances for these catalysts were monitored for the oxidative degradation of phenol and the results are shown in Table 2. 88% degradation of phenol was achieved with the pure TiO_2 catalysts under UV light irradiation for 90 min. The degradation ability for the binary oxide catalysts (TiO_2–ZrO_2) increased with an increase in the amount of TiO_2 or ZrO_2 loadings to ZrO_2 or TiO_2 (Table 2). The 50 wt% TiO_2 showed the highest percentage of phenol degradation (100%), however, after that weight percentage, there was noticeable change in the reactivity and the value remained the same with further loadings of TiO_2 (Table 2). Also, phenol degradation decreases from 100 to 56% with the 10 wt% ZrO_2 mixed with TiO_2.

In fact, the catalytic activity of 50 wt% TiO_2 to ZrO_2 was found to be higher than the standard Degussa TiO_2 P-25 photocatalyst. Fu et al. have reported that, after 12 wt% ZrO_2 loading to TiO_2, the catalytic activity slowly decreased (ZrO_2–TiO_2) until zero for the pure

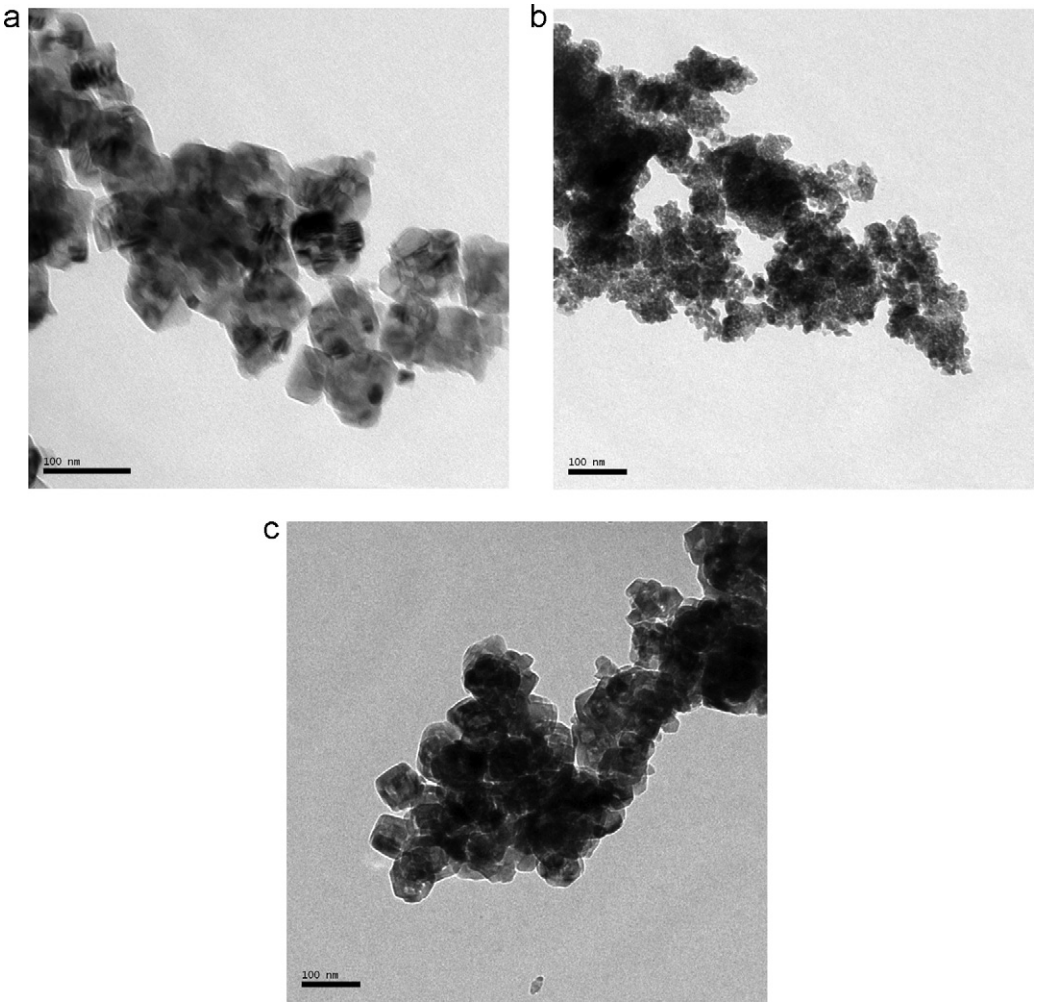

Fig. 4. TEM pattern of (a) TiO_2 (b) ZrO_2, (c) %50 TiO_2–ZrO_2 prepared by SSD method.

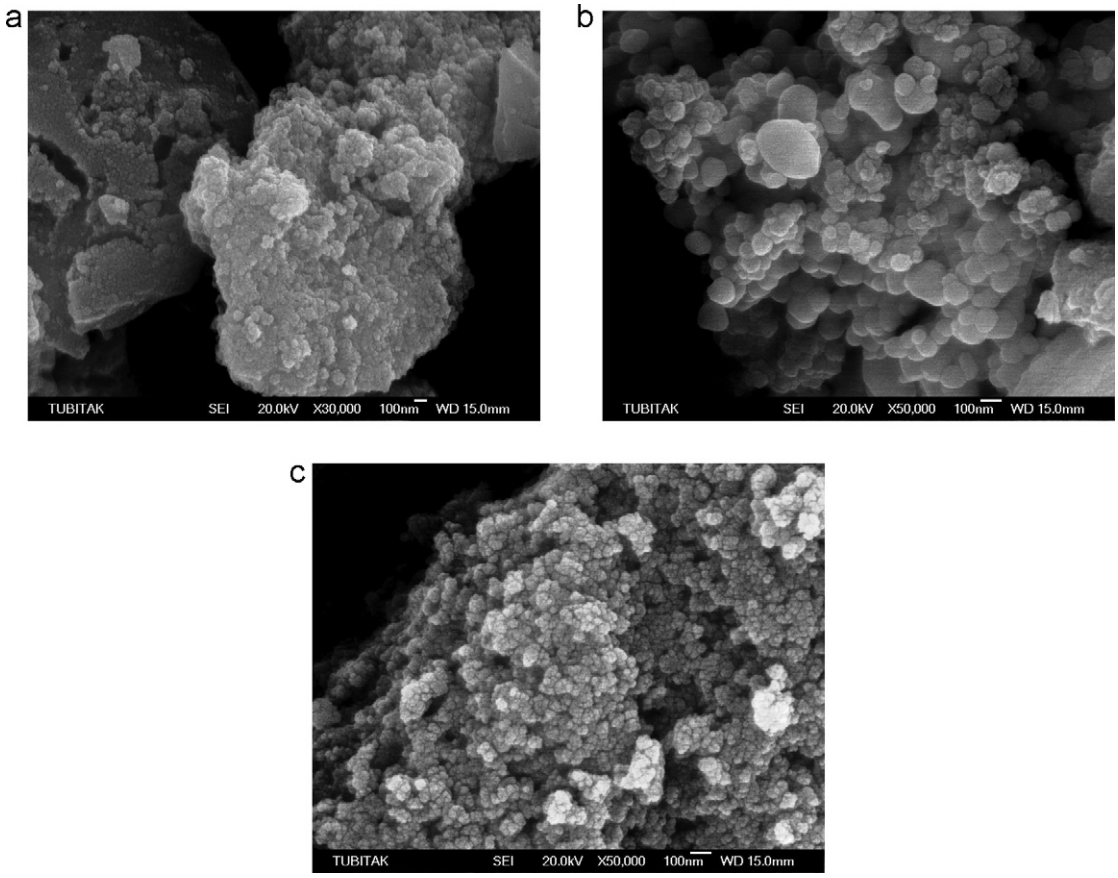

Fig. 5. SEM pattern of 50% TiO_2–ZrO_2 (a) impregnation, (b) sol–gel, (c) SSD method.

ZrO_2 [18]. However, in this study, pure ZrO_2 contributed 52% phenol degradation in 5 h. Although the ZrO_2 band gap is high (4.6 eV), ZrO_2 itself can act as a photocatalyst. Zirconia is substantially less active than titania. For photocatalytic oxidation of isopropanol, photocatalytic activities (mmol h^{-1}) were obtained ZrO_2 (Degussa), ZrO_2 (home-prepared) and TiO_2 are 1.63, 1.41 and 15.0, respectively [26].

The activity results revealed that TiO_2–ZrO_2 binary oxides exhibited mixed tetragonal and monoclinic phases of ZrO_2. The photocatalytic activity is influenced by the amount of the monoclinic phase. It is clearly seen that the activity varies in parallel with the amount of monoclinic phase. The catalytic activity of the binary oxide catalysts gradually increased with an increase in the amount of monoclinic phase for a lower amount of TiO_2 (20–50 wt%). However, after 50 wt%, there was a decrease in the reactivity in parallel with the amount of monoclinic phase for a higher amount of TiO_2 (70–90 wt%).

And also photocatalytic activities of 50TiO_2–ZrO_2 binary oxide catalyst prepared by different methods were shown in Fig. 8. The catalyst prepared with sol–gel method showed the lowest activity. The conversion of phenol has reached to 35%

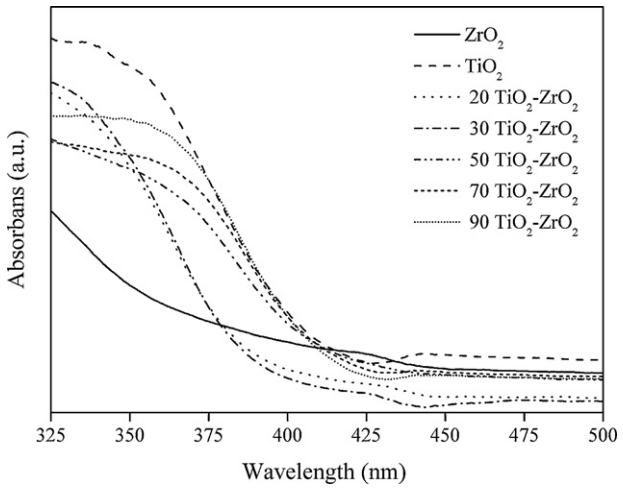

Fig. 6. UV–vis diffuse reflectance spectra of samples.

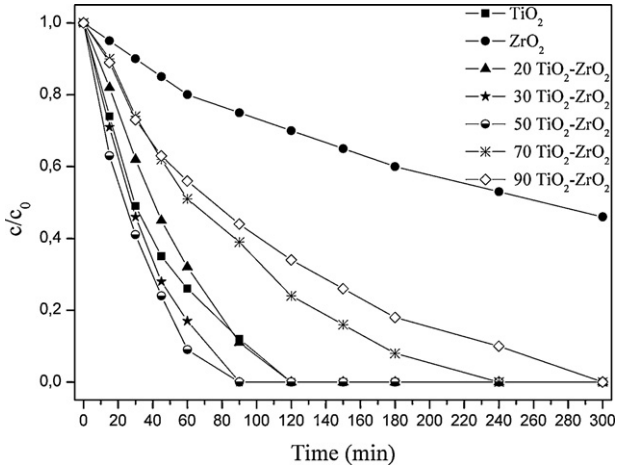

Fig. 7. Photodegradation of phenol on TiO_2, ZrO_2 and TiO_2–ZrO_2 binary oxide catalysts.

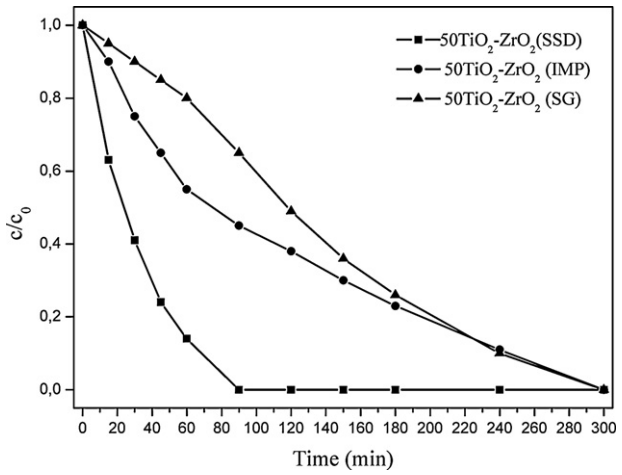

Fig. 8. The influence of catalyst preparation technique on photocatalytic activity of phenol by $50TiO_2$–ZrO_2 binary oxide catalyst.

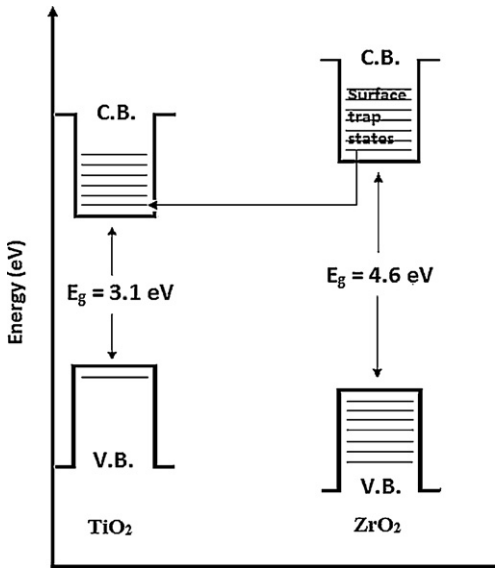

Fig. 9. Schematic energy level diagram of interparticle electrons transfer process between and TiO_2 ZrO_2 in TiO_2–ZrO_2 binary oxide catalysts.

at the end of the 90 min by using the $50TiO_2$–ZrO_2 (SG). The observed photodegradation activity for phenol follows the order $50TiO_2$–ZrO_2(SSD) > $50TiO_2$–ZrO_2(IMP) > $50TiO_2$–ZrO_2(SG). This result may show that tetragonal phase of ZrO_2 may not improve the photodegradation. Based on the XRD patterns of catalysts, the presence of monoclinic phase of ZrO_2 is more effective in photodegradation reactions.

This high photoactivity may be due to the abundance of hydroxyl groups present on the catalyst surface, which can prevent the electron–hole recombination by trapping hole and generating OH radicals acting as powerful oxidants. This has been proved by the FTIR experiments. Similar results were observed by Neppolian et al. [27].

The activity of the photocatalyst is influenced by its crystallinity as well as other factors such as surface area, crystal size, synthesis method, band gap, crystal phase and surface OH group.

When a lower amount of ZrO_2 (10–50 wt%) was loaded to TiO_2 the catalytic activity of the binary oxide catalysts gradually increased with an increase in the amount of ZrO_2 loading, however, after 50 wt%, there was a decrease in the reactivity. Although the small amount of surface OH groups appeared in the FTIR from 70 to 80 wt% ZrO_2, obtained high surface area and small crystallite sizes (particle size), the catalytic activity slowly decreased. Moreover, a lower amount of (20–50) wt% TiO_2 to ZrO_2 showed high activity despite the decrease in surface area and increase in crystallite size (particle size).

According to activity results, the surface area, particle size and surface OH groups were not the only contribution in high reactivity for the degradation of phenol. The reaction with the binary oxide catalysts is more important beside the surface area, particle size and surface OH groups. The optimum photodegradation activity was seen 50 wt% ZrO_2–TiO_2. Our XRD observations clearly show that Ti is in interaction with the Zr.

Neppolian et al. expressed that electron injection was shown to be the major factor in the high activity of the binary oxide catalysts along with other physicochemical characteristics. The transfer of electrons from ZrO_2 to TiO_2 was seen to the main phenomena in the binary oxide catalyts through chemical interactions between ZrO_2 and TiO_2 in the form of the Ti—O—Zr— bond [27].

In addition, Wu et al., have described the formation of a mutual chemical interaction between the pure oxides when they are co-precipitated together (—Ti—O—Zr—), leading to a profound effect on the photocatalytic properties [28].

As reported by Fu et al., electron and hole separation may take place between ZrO_2 and TiO_2 in the binary oxide [18] since the energy level of TiO_2 both for the valence band and conduction band correspond well within the band gap of ZrO_2, as shown in Fig. 9. When the electrons are excited from both catalysts, most of the electrons from the conduction band (CB) of ZrO_2 can easily transfer to the CB of TiO_2 and, thereby, the electron–hole recombination may be prevented in ZrO_2 (10–50 wt%) loaded to TiO_2. In the case of TiO_2 (20–50 wt%) loaded to ZrO_2, a greater the number of electrons may be excited from the valence band (VB) of ZrO_2 to the CB of ZrO_2 in comparison to pure TiO_2 but less electrons may be transferred to the CB of TiO_2 since the loaded amount of TiO_2 is less than ZrO_2 [27].

Kamat and Sant have reported the preparation of CdS–TiO_2 nanoclusters photocatalysts in which the bottom of the conduction band of TiO_2 is lower than that of CdS by 0.5 eV, the driving force facilitating the easy transfer of electrons from the CB of CdS to the CB of TiO_2 [29]. This is proved by comparing the emission spectra of the pure and coupled TiO_2 and CdS nanoclusters in which significant quenching of the CdS emission is observed by the addition of TiO_2. Similarly, in these binary oxide catalysts, the bottom of the CB edge of ZrO_2 is around 1.3 eV higher than that of TiO_2, as reported by Ghosh and co-workers [30]. Hence, there may be a fast transfer of the photo-formed electrons from the CB of ZrO_2 to that of TiO_2, preventing radiative photo-formed electron–hole recombination. Electrons may be transferred to the CB of TiO_2 since the loaded amount of TiO_2 is less than ZrO_2 [26].

It can be seen from Table 2 that the pure nano-TiO_2 possessed the surface area of 40 m^2/g. With 50 wt% ZrO_2–TiO_2 catalyst, the specific surface area increased to 66 m^2/g, which was higher than that of the Degussa P25 (50 m^2/g). Wang and Fan reported that the higher surface areas and pore volumes had more surface active sites and channels that allowed the rapid diffusion of various liquid reactants and products during the photocatalytic reaction and thus, increasing the photodegradation rate of reaction [31,32].

In our study, 50 wt% ZrO_2–TiO_2 compared to nano-TiO_2 (synthesized) and Degussa P25 exhibited superior photocatalytic activity. It has high photocatalytic activity because of the high specific surface area and smaller particle size. SNTZS photocatalyst, prepared different ZSM-5 loading (from 0.1 to 0.9 g/L), synthesized using the modified sol–gel method. According to BET results, the surface area

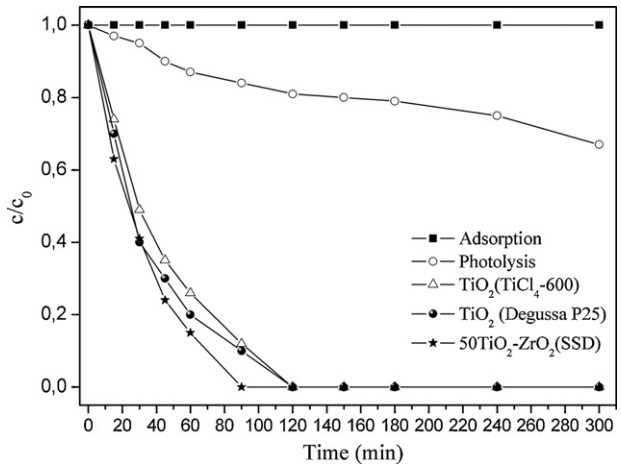

Fig. 10. Time course of the adsorption of phenol by $50TiO_2$–ZrO_2(SSD) in dark, the photolysis of phenol, and the degradation of phenol by $50TiO_2$–ZrO_2(SSD) under UV irradiation.

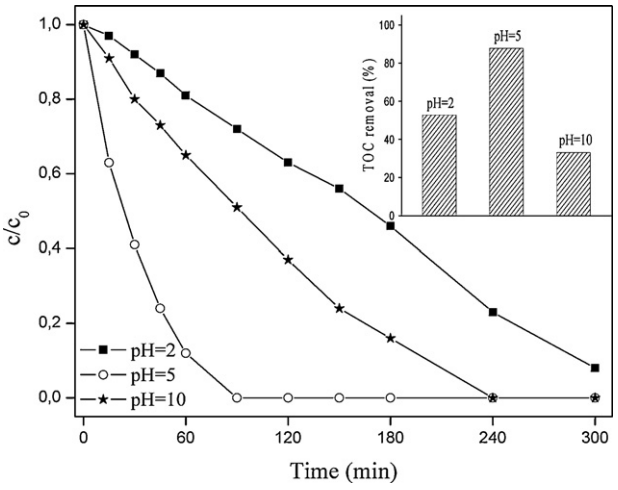

Fig. 11. The influence of pH on the photocatalytic degradation of phenol on $50TiO_2$–ZrO_2 (SSD). Inset shows the impact of pH on TOC removal in the phenol degradation by the $50TiO_2$–ZrO_2 (SSD) sample.

was reduced from 0.3 g/L (optimum composition). 0.3 g/L for SNTZS showed better photocatalytic activity compared to the Degussa P25. Besides, the optimum composition of SNTZS has smaller particle size, 8–22 nm compared to Degussa P25, 21.3 nm which in turn showing faster phenol degradation than Degussa P25 [33].

The adsorption (dark experiment), photolysis (experiment under illumination and no catalyst) and photodegradation (experiment under illumination) of phenol on $50TiO_2$–ZrO_2(SSD) are shown in Fig. 10. It can be clearly seen that the adsorption of phenol on the surface of $50TiO_2$–ZrO_2(SSD) material is negligible. The photolysis of phenol under the UV irradiation is about 19% in 2 h. $50TiO_2$–ZrO_2(SSD) sample exhibits a much higher efficiency in degradation of phenol than pure TiO_2 and Degussa-P25. It has been found by some researchers that the Degussa-P25 has a higher photocatalytic activity than that of any other catalysts of the similar grade [34,35]. Saravanan et al. [36] studied the degradation of phenol in the presence of sunlight with Degussa P-25 and Anjatox TiO_2. Anjatox was capable of completely degrading at initial phenol concentration of 50 mg/L within 7 h. On the other hand, Degussa P-25 catalyst required only 5 h for complete degradation. Nevertheless, concentrations above 50 mg/L were not completely degraded at all by using either of the two photocatalysts even after 10 h. According to the studies reported by Zainudin et al. [33], SNTZS (the mixture of nano-TiO_2 and ZSM-5 supported on silica gel) and Degussa P25 exhibited 90 and 67% of phenol degradation after 180 min, respectively.

Fig. 11 presents the influence of pH on the photocatalytic degradation of phenol on $50TiO_2$–ZrO_2 prepared by SSD method. The initial pH of the phenol solution is altered by HNO_3 and NaOH solutions. The results of Fig. 11 indicate that photodegradation of phenol is not favored in an acidic solution (pH < 5). The degradation efficiency reaches a maximum at pH 5 (natural pH). 25 ppm phenol can be completely degraded in 90 min by $50TiO_2$–ZrO_2 (SSD) sample at an initial pH of 5 and 90% TOC removal can be achieved in 90 min. This result emphasizes the achievement of the total mineralization. However, the TOC removal was reached to 81% with the Degussa P25, which can be completely degraded in 2 h.

The photocatalytic degradation rate decrease at a higher pH of 10. Phenol tends to exist as phenolate anions at higher pH values. On the other hand, the decreased photocatalytic degradation rate from pH 5 to 10 probably resulted from the repulsive force between them [37]. Similar results were also reported by some researchers [38,39]. The initial pH obviously plays a complex role on influencing the degradation of phenol. In alkaline solution, a higher concentration of hydroxide ions (OH^-) are available around the catalyst surface for reaction with photogenerated holes in comparison with acidic condition, which will result in the more efficient formation of hydroxyl radicals. Since hydroxyl radicals are important oxidizing species in the photocatalytic process, the photocatalytic degradation of phenol may be accelerated in alkaline solution. However, the catalyst shows an amphoteric behavior in aqueous medium. Electric charge properties of both, catalyst and substrate, are found to play an important role on adsorption process. The point of zero charge (pzc) is determined by procedure indicated in Ref. [40]. The surface of catalyst will be negatively charged at pH higher than pzc but positively charged at lower pH values [41]. For Degussa P-25 TiO_2 used here, the point of zero charge is between 6.25 and 6.60 [39,41].

HPLC analysis performed during the photocatalytic runs. Catechol (CT; 2-hydroxyphenol) and hydroquinone (HQ; 4-hydroxyphenol) were detected as main intermediates. And also ring-opening products are supposed to be short chain acids, such as, acetic acid, maleic acid, oxalic acid, etc. [42], they were identified by GC–MS analysis.

The results of HPLC studies of photocatalytic reaction show phenol concentration decays following a pseudo first order rate law, reaching at the end of the photocatalytic run essentially zero concentration and the concentration of the main reaction intermediates initially rise and then decrease until almost complete disappearance at the same time of complete phenol conversion. Concentration profiles for phenol, catechol and hydroquinone obtained during the photocatalytic oxidation reaction using $50TiO_2$–ZrO_2(SSD) is shown in Fig. 12a. Besides, the distribution of intermediates was also compared in different binary oxide catalysts. According to HPLC results, the concentration of catechol gradually increased with an increase in the amount of ZrO_2 loading to TiO_2. However, the concentration of hydroquinone showed slowly increased with an increase in the amount of ZrO_2 loading, however, after 50 wt%, there was a decrease in the concentration. Moreover, when a higher amount of ZrO_2 (80 wt%) was loaded to TiO_2, it was observed that the concentration of catechol was slightly higher than the concentration of hydroquinone.

The results of HPLC studies of photocatalytic reaction show phenol concentration decays following a pseudo first order rate law, reaching at the end of the photocatalytic run essentially zero concentration and the concentration of the main

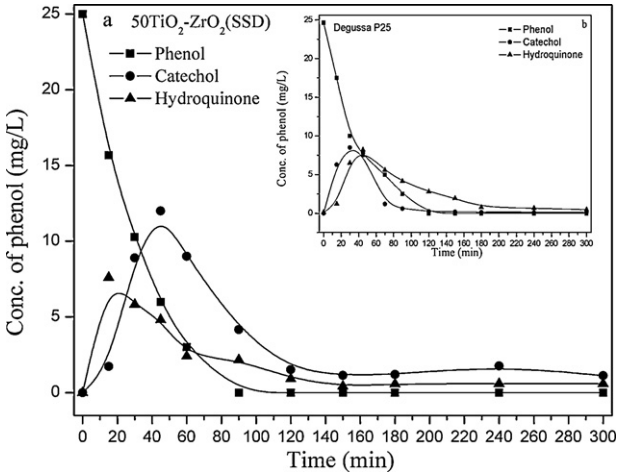

Fig. 12. Concentration profiles for phenol, catechol and hydroquinone obtained during the photocatalytic oxidation reaction using (a) $50TiO_2$–ZrO_2(SSD) (b) Degussa P25.

reaction intermediates initially rise and then decrease until almost complete disappearance at the same time of complete phenol conversion. Concentration profiles for phenol, catechol and hydroquinone obtained during the photocatalytic oxidation reaction using $50TiO_2$–ZrO_2(SSD) is shown in Fig. 12a. Besides, the distributions of intermediates also were compared in different binary oxide catalysts. According to HPLC results, the concentration of catechol gradually increased with an increase in the amount of ZrO_2 loading to TiO_2. However, the concentration of hydroquinone showed slowly increased with an increase in the amount of ZrO_2 loading, however, after 50 wt%, there was a decrease in the concentration. Moreover, when a higher amount of ZrO_2 (80 wt%) was loaded to TiO_2, it was observed that the concentration of catechol was slightly higher than the concentration of hydroquinone.

Conversion of phenol to catechol is likely to be more advantageous for the complete mineralization of phenol than conversion to BQ (benzoquinone) or HQ (4-hydroxyphenol), as reported by Santos et al. [43], because catechol is decomposed to oxalic acid, and then to CO_2 and water, whereas the pathways of mineralization of BQ and HQ are much longer.

Similar to the $50TiO_2$–ZrO_2 binary oxide catalyst, catechol and hydroquinone were detected as main intermediates by using Degussa P-25. Fig. 12b shows the phenol decomposition on Degussa P-25. It can be seen that the highest yield was for hydroquinone in 2 h. It is noteworthy to mention that, catechol for the Degussa P-25 was found in lower concentration compared to 50–TiO_2–ZrO_2. It should be noted that, some structural features of catalyst play a significant role during the photocatalysis.

4. Conclusions

From these results on preparation, characterization and evaluation of TiO_2–ZrO_2 catalysts for the photodegradation of phenol, we may explain the use of ZrO_2 and SSD method in enhancing the photodegradation activity.

The 50 wt% TiO_2 showed the highest percentage of phenol degradation (100%) and highest reaction rate (0.73 mg L^{-1} min^{-1}). Also, the catalytic activity of $50TiO_2$–ZrO_2 was found to be higher than the standard Degussa TiO_2 P-25 photocatalyst. The chemical interaction between TiO_2 and ZrO_2 in the form of the Ti—O—Zr— bond may affect the photoefficiency of binary oxide catalysts.

The profound effect of $50TiO_2$–ZrO_2(SSD) binary oxide catalyst for phenol degradation is generally considered due to the high surface area, small particle size, anatase phase and high monoclinic phase of ZrO_2 content, and the presence of more surface OH groups than that of the pure TiO_2 and ZrO_2 photocatalysts.

The catalytic activity was affected by the preparation method. Comparatively, the phenol degradation over $50TiO_2$–ZrO_2(SG) after 90 min was 35%. The observed photodegradation activity for phenol follows the order $50TiO_2$–ZrO_2(SSD) > $50TiO_2$–ZrO_2(IMP) > $50TiO_2$–ZrO_2(SG). Monoclinic form of ZrO_2 is more effective for photodegradation.

A natural pH of 5 is favorable for the photodegradation of phenol by $50TiO_2$–ZrO_2(SSD) and 90% TOC removal can be achieved in 90 min. Hydroquinone and catechol are detected as the main intermediates resulting from the attack of hydroxyl radical in the *para* and *ortho* positions of phenol molecule, respectively.

Acknowledgment

This work was supported by the Research Fund of the Istanbul University.

References

[1] C. Baird, Environmental Chemistry, Freeman, New York, 1998.
[2] N. Serpone, R. Terzian, C. Minero, E. Pelizzetti, American Chemical Society, Washington, 1993.
[3] J.-C. D'Oliveira, G. Al-Sayyed, P. Pichat, Environ. Sci. Technol. 24 (1990) 990.
[4] M.R. Hoffmann, S.T. Martin, W.Y. Choi, D.W. Bahnemann, Chem. Rev. 95 (1995) 69–96.
[5] L. Palmisano, V. Augugliaro, A. Sclafani, M. Schiavello, J. Phys. Chem. 92 (1988) 6710–6713.
[6] J.C. Yu, J.G. Yu, W.K. Ho, Z.T. Jiang, L.Z. Zhang, Chem. Mater. 14 (2002) 3808–3816.
[7] W.Y. Choi, A. Termin, M.R. Hoffmann, J. Phys. Chem. 98 (1994) 13669–13679.
[8] F.B. Li, X.Z. Li, Appl. Catal. A 228 (2002) 15–27.
[9] Y. Liu, C.Y. Liu, Q.H. Rong, Z. Zhang, Appl. Surf. Sci. 220 (2003) 7–11.
[10] M. Asilturk, F. Sayilkan, E. Arpac, J. Photochem. Photobiol. A 203 (2009) 64–71.
[11] L.G. Devi, B.N. Murhty, S.G. Kumar, Catal. Lett. 130 (2009) 496–503.
[12] M.D. Hernandez-Alonso, J.M. Coronado, B. Bachiller-Baeza, M. Fernandez-Garcia, J. Soria, Chem. Mater. 19 (2007) 4283–4291.
[13] V. Vishwanathan, H.-S. Roh, J.-W. Kim, K.-W. Jun, Catal. Lett. 96 (2004) 23–28.
[14] K.V.R. Chary, G.V. Sagar, D. Naresh, K.K. Seela, B. Sridhar, J. Phys. Chem. B 109 (2005) 9437–9444.
[15] C. Wu, X. Zhao, Y. Ren, Y. Yue, W. Hua, Y. Cao, Y. Tang, Z. Gao, J. Mol. Catal. A 229 (2005) 233–239.
[16] J.A. Navio, M.C. Hidalgo, G. Colon, S.G. Botta, M.I. Litter, Langmuir 17 (2001) 202–210.
[17] X.Wang, J.C. Yu, Y. Chen, L.Wu, X. Fu, Environ. Sci. Technol. 40 (2006) 2369–2374.
[18] X. Fu, L.A. Clark, Q. Yang, M.A. Anderson, Environ. Sci. Technol. 30 (1996) 647–653.
[19] H. Toyara, M. Yoshimura, S. Somiya, J. Am. Ceram. Soc. 67 (6) (1984) 119–121.
[20] J.C. Yu, J. Lin, R.W.M. Kwok, J. Phys. Chem. B 102 (1998) 5094–5098.
[21] Y.A. Cao, W.S. Yang, W.F. Zhang, G.Z. Liu, P.L. Yue, New J. Chem. 28 (2004) 218–222.
[22] C. Anderson, A.J. Bard, J. Phys. Chem. B 101 (1997) 2611–2616.
[23] L. Wu, J.C. Yu, L. Zhang, X. Wang, W. Ho, J. Solid State Chem. 177 (2004) 2584–2590.
[24] S. Sakthivel, M.C. Hidalgo, D.W. Bahnemann, S.U. Geissen, V. Murugesan, A. Vogelpohl, Appl. Catal. B: Environ. 63 (2006) 31–40.
[25] Y.M. Xu, C.H. Langford, J. Photochem. Photobiol. A 133 (2000) 67.
[26] J.A. Navio, G. Colon, J.M. Herrmann, J. Photochem. Photobiol., A: Chem. 108 (1997) 179–185.
[27] B. Neppolian, Q. Wang, H. Yamashita, H. Choi, Appl. Catal. A: Gen. 333 (2007) 264–271.
[28] J.-C. Wu, C.-S. Chung, C.-L. Ay, I. Wang, J. Catal. 87 (1984) 98–107.
[29] P.A. Sant, P.V. Kamat, Phys. Chem. Chem. Phys. 4 (2002) 198–203.
[30] G. Ramakrishna, A.K. Singh, D.K. Palit, H.N. Ghosh, J. Phys. Chem. B 108 (2004) 4775–4783.
[31] Z. Wang, W. Cai, X. Hong, X. Zhao, F. Xu, C. Cai, Appl. Catal. B 57 (2005) 223–231.
[32] X. Fan, X. Chen, S. Zhu, Z. Li, T. Yu, J. Ye, Z. Zou, J. Mol. Catal. A: Chem. 284 (2008) 155–160.
[33] N.F. Zainudin, A.Z. Abdullah, A.R. Mohamed, J. Hazard. Mater. 174 (2010) 299–306.
[34] L. Zhang, T. Kanki, S. Norikai, A. Toyada, Sol. Energy 70 (2001) 331–337.
[35] D. Vione, C. Minero, V. Maurino, M.E. Carlotti, T. Picatonotto, E. Pelizzetti, Appl. Catal. B: Environ. 58 (2005) 79–88.
[36] P. Saravanan, K. Pakshirajan, P. Saha, J. Hydro-Environ. Res. 3 (2009) 45–50.

[37] I.K. Konstantinou, T.A. Albanis, Appl. Catal. B: Environ. 49 (2004) 1–14.
[38] C. Chiou, C.-Y. Wu, R.-S. Juang, Chem. Eng. J. 139 (2008) 322–329.
[39] T.Y. Wei, Y.Y. Wang, C.C. Wei, J. Photochem. Photobiol. A: Chem. 55 (1991) 115–126.
[40] J. Rivera-Utrilla, I. Baustista-Toledo, M.A. Ferro-Garcia, C. Moreno-Castilla, J. Chem. Technol. Biotechnol. 76 (2001) 1209–1215.
[41] R.A. Doong, C.H. Chen, R.A. Maithreepala, S.M. Chang, Water Res. 35 (2001) 2873–2880.
[42] B. Tryba, A.W. Morawski, M. Inagaki, M. Toyoda, Appl. Catal. B: Environ. 63 (2006) 215–221.
[43] A. Santos, P. Yustos, A. Quintanilla, S. Rodriguez, F. Garcia-Ochoa, Appl. Catal. B: Environ. 39 (2002) 97.